Frontiers of Physics
https://doi.org/10.1007/s11467-019-0928-x
Front. Phys.
15(1), 12601 (2020)

RESEARCH ARTICLE

Electromagnetically induced transparency in novel dual-band metamaterial excited by toroidal dipolar response

Zhao-Yang Shen[1], He-Lin Yang[1,†], Xuan Liu[3], Xiao-Jun Huang[2], Tian-Yu Xiang[1,4], Jiong Wu[1], Wei Chen[1]

[1] *College of Physical Science and Technology, Central China Normal University, Wuhan 430079, China*
[2] *College of Communication and Information Engineering, Xi'an University of Science and Technology, Xi'an 710054, China*
[3] *School of Computer and Information, China Three Gorges University, Yichang 443002, China*
[4] *School of Mechanical and Electrical Engineering, Guizhou Normal University, Guiyang 550000, China*
Corresponding author. E-mail: [†] *emyang@mail.ccnu.edu.cn*
Received July 12, 2019; accepted September 10, 2019

We demonstrated a novel metamaterial with dual-band electromagnetically induced transparency (EIT) via simulation, experiment and numerical analysis, with resonance frequencies of the transparency peaks of 7.60 and 10.27 GHz. The E–ε metamaterial unit cells were composed of E-shaped and ε-shaped patterns. By analyzing the surface current distribution and the magnetic field, we qualitatively verified the toroidal dipole response in the E–ε metamaterial at 10.27 GHz. Meanwhile, by calculating the multipole's radiated power, we found that the two transparency peaks were due to the excitation of the electric and toroidal dipole responses. By changing the incident angle from 0° to 60°, we observed changes in transmission spectra, and the quality factors (Q-factors) of the two transparency peaks increased. In addition, the proposed E–ε metamaterial can be designed to act as a refractive index sensor or other electronic equipment for the control of electromagnetic waves.

Keywords metamaterial, dual band electromagnetically induced transparency, toroidal dipole response

1 Introduction

Metamaterials are artificial materials [1, 2] that have a variety of special physics phenomena, including negative refraction [3], reversals of both Doppler shift and Cherenkov radiation [4], perfect absorption [5], and super lenses [6]. These phenomena cannot be found in natural materials. Owing to these properties, metamaterials have an amount of applications in civilian and military products such as electromagnetic compatibility (EMC) [7], frequency selective surface (FSS) [8], sensors [9], transformation optics [10, 11], and invisibility cloaks [12]. The electromagnetic response in metamaterials is referred to as the electromagnetic multipole. The electric and magnetic multipoles play significant roles in the electromagnetic multipole family. However, as a third family, the toroidal multipole [13] is negligible because of the other multipoles' strong excitation. The toroidal dipole was first proposed by Zel'dovich [14]. The formation of a toroidal dipole can be introduced by a current flow on a toroidal surface along its meridian. A distinct feature of toroidal metamaterials, anapole excitation, is of nontrivial, nonradiating nature [15]. Recently, research surrounding toroidal dipoles in metamaterials has become popular and has shown many unusual properties, including polarization conversion [16], unconventional optical activity [17] and resonance transmission [18].

Electromagnetically induced transparency (EIT) [19, 20] is a three-level quantum interference process in an atomic system. When the different energy level coupling, the transmission spectrum forms a sharp transparency peak at a specific frequency. However, achieving the EIT phenomena needs a series of strict environmental conditions (a low-temperature, high-intensity optical pump) in experimental circumstances. Metamaterials provide convenience for researchers to realize EIT without difficult setups. The EIT phenomena has supported by considerable research from microwave, optics, near-infrared [21], etc. The EIT metamaterial has many potential applications, for example, the sensing of dielectric media and biomolecules [22], refractive index sensors [23] and optical switches [24]. The bright-dark mode coupling [25, 26] is the most basic method to acquire a classical EIT phenomenon. Generally, the bright mode can be directly excited by an incident electromagnetic wave and has a low quality factor (Q-factor). Therefore, the bright mode can be seen as the electric dipole response. By contrast, the dark mode is weakly radiated by an electromagnetic wave and has a high Q-factor, which serves as the magnetic dipole response.

© Higher Education Press and Springer-Verlag GmbH Germany, part of Springer Nature 2020

In recent years, many researchers have paid more attention to EIT and Fano resonance [27] in metamaterials with the toroidal dipole response. In 2013, Fedotov *et al.* [28] proposed four dumbbell-shaped apertures in a thin metal plate, constituting a compass-shaped cross-section element, which created destructive interference between the toroidal and electric dipoles and acquired symmetric Lorentzian transparency lines. Guo *et al.* proposed an electric toroidal dipole that etched a sun-like aperture metal pattern at Rogers 4003C in 2014 [29]. In 2015, Han *et al.* [30] observed Fano resonance and EIT in a three-dimensional toroidal metamaterial that consisted of three identical combine split resonance ring by sharing a central connecting bridge, forming a hexagon. The first demonstration of toroidal excitation in 2D metamaterials was shown by Gupta *et al.* [31] in 2016. The setup consisted of two joint metallic loops with two capacitive gaps in each loop. Zhu *et al.* [32] employed a type-I cut wire and two spiral ring resonators to achieve a planar toroidal metamaterial in 2017. This work indicated that EIT could be attributed to the coupling between the electric and toroidal dipoles. In 2018, the classical Ising model was used to verify Fano resonance with strong magnetic and toroidal dipole responses, which was proposed by Cong *et al.* [33].

A planar dual-band EIT E–ε metamaterial is proposed, named so as it consists of E- and ε-shaped structures, with transparency peaks located at 7.60 and 10.27 GHz. The simulation and experimental results are seen to be consistent. The calculation results of the radiated power multipoles show that the toroidal dipole response is weaker than the electric dipole response at 7.60 GHz and stronger than the electric dipole response at 10.27 GHz. This phenomenon could be explained by the surface current distribution and the magnetic field. With increasing incident and polarizing angles, the transmission spectra change, and the Q-factors of the two transparency peaks increase. The proposed E–ε metamaterial can be used in refractive index sensors.

2 Design, simulation, and experiment

The unit cell structure is made up of two parts: E-shaped and ε-shaped metal patterns. The CST Microwave Studio simulation software is used to obtain simulation results, in which the x- and y-axes are set as unit cell boundaries and the z-direction is an open space (add). The geometrical parameters of the two different unit cell structures are shown in Fig. 1(a). The dielectric slab is 1 mm-thick F4B with permittivity and loss tangents of 2.2 and 0.001. The metal pattern is formed of 0.035 mm-thick copper with a conductivity of 5.96×10^7 S/m. Fig. 1(b) shows the transmission spectra of the E-shaped pattern, in which the dip of the transmission coefficient was -46.65 dB at 8.07 GHz. The transmission spectra of the ε-shaped pattern are shown in Fig. 1(c), where the frequency of the

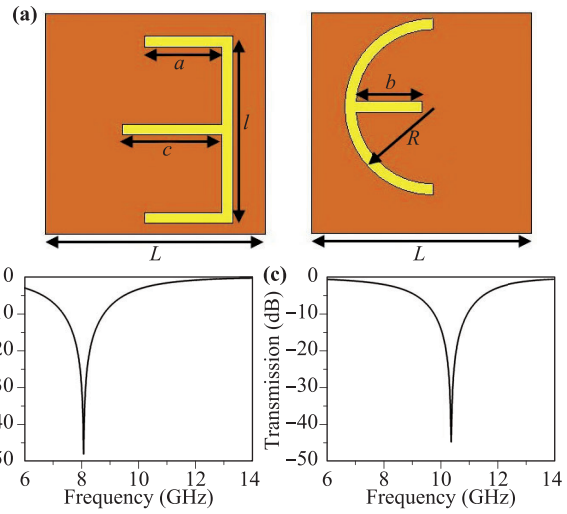


Fig. 1 **(a)** The unit cells of the E-shaped and ε-shaped patterns, with geometrical parameters $L = 10$ mm, $l = 8.5$ mm, $R = 4$ mm, $a = 4$ mm, $b = 3$ mm, $c = 4.5$ mm and metal width = 0.5 mm. **(b)** The transmission spectrum of the E-shape. **(c)** The transmission spectrum of the ε-shape.

transmission dip was 10.34 GHz with a -44.70 dB transmission coefficient. The Q-factors were 3.34 (Q_{E}) for the E-shaped pattern at 8.07 GHz and 6.01 (Q_{ε}) for the ε-shaped pattern at 10.34 GHz, which were solved by using the formula $Q = f/FWHM$, where f is the resonance frequency and $FWHM$ is the full width at half maximum bandwidth. The transmission spectra of the E-shape show a line at 10.34 GHz, and the transmission coefficient approximates to 0 at 8.07 GHz for the ε-shape. Therefore, the E-shaped structure shows bright-mode coupling for the low frequency and dark-mode coupling for the high frequency.

In order to achieve EIT, the unit cell comprises two mirrored and interlocked E- or ε-shaped patterns. However, the transmission spectra only appear one transparency peak in two different metamaterials, as shown in Fig. 2. The transparency peak was located at 8.59 GHz, with a transmission coefficient of -3.70 dB, as shown in Fig. 2(a), for the mirrored E-shaped pattern. The transmission spectrum of the mirrored asymmetric ε-shapes is shown in Fig. 2(b), with the transparency peak appearing at 13.35

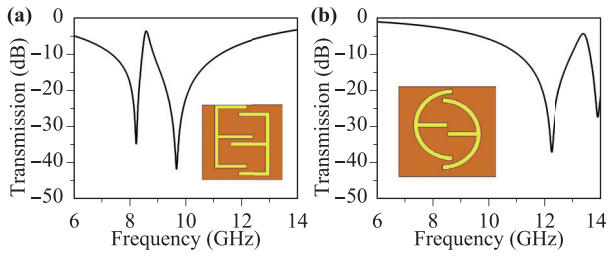


Fig. 2 Transmission spectra of the mirrored, asymmetric structures: **(a)** E-shaped and **(b)** ε-shaped.

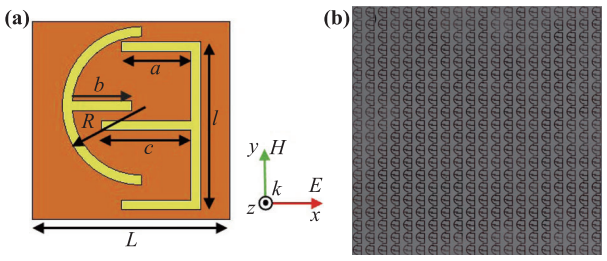


Fig. 3 **(a)** The image of the metamaterial's unit cell structure. **(b)** Photograph of the fabricated sample.

GHz with a transmission coefficient of −4.37 dB.

Using the above simulation results, the dual-band EIT metamaterial can be realized by combining the E-shape and the ε-shape in a single unit cell, as shown in Fig. 3(a). The geometrical parameters of this setup are the same as those in Fig. 1. The 200 mm × 200 mm sample was fabricated using a printed circuit board, and its image is shown in Fig. 3(b). The experimental results are measured using a vector network analyzer (Agilent PNA E8362B) and a pair of horn antennas in free space.

Figure 4 shows the transmission spectra of the E–ε metamaterial from the simulation and experiment results. In the simulation, there were two transparency peaks located at 7.60 and 10.27 GHz, with corresponding transmission coefficients of −0.31 and −0.49 dB, as well as three transmission dips at 7.22, 9.66, and 11.83 GHz, with corresponding transmission coefficients of −33.77, −41.42, and −43.01 dB. In the experiment, the resonance frequencies of two transparency peaks were 7.67 and 10.25 GHz, for which the transmission coefficients were −0.16 and −0.85 dB. This agrees well with the simulation results. However, the three transmission dips were found to be at 7.30, 9.73, and 11.76 GHz, which deviates from the values found via simulation. Their transmission coefficients were −23.24, −32.93, and −29.41 dB, respectively. There are two main factors causing the disparity between the simulation and experiment. Firstly, the permittivity or loss tangle of the dielectric slab in the experiment has a little discrepancy compared to that in the simulation, and second is the presence of strong electromagnetic wave diffraction at a higher frequency.

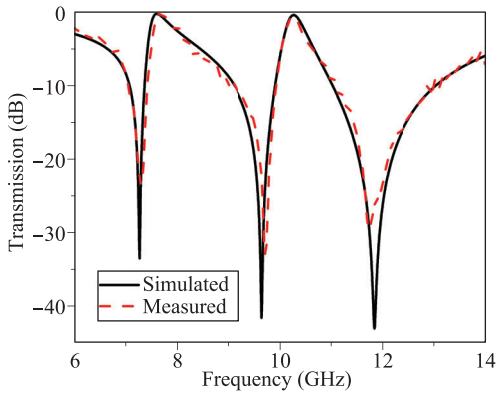


Fig. 4 Simulated and measured transmission spectra of the E–ε metamaterial.

3 Results and discussion

To further probe the characteristics of the EIT E–ε metamaterial, we verify a variety of transmission spectra with different incident (θ) and polarizing angles (φ) by numerical simulation and experimental measurement. Fig. 5(a) shows the simulation results for the different incident angles (θ), which changed from 0° to 60° with a step of 15°. When the incident angle rose from 0° to 45°, the four curves of transmission spectra became almost identical. The width of the two transmission windows decreases at an incident angle of 60°. However, the resonance frequencies of the two transparency peaks remain at 7.60 and 10.27 GHz. The Q-factors of the two transparency peaks are presented in Table 1 and are shown to increase with the incident angle. The experimental results are shown in Fig. 5(b). The resonance frequencies of the two transparency peaks perfectly coincide with the simulation results, which are 7.67 and 10.25 GHz. When the incident angles change from 0° to 60°, the variation of the transmission windows is nearly identical, and the width of the transmission windows decreases.

The simulated and measured results with different polarizing angles φ are presented in Fig. 6. The polarizing angles ranged from 0° to 45° with a step of 15°. The amplitude of the transmission dips gradually increased, and the resonance frequencies became blue-shifted, as shown in Fig. 6(a). For instance, in the second transmission dip, the transmission coefficient was −41.42 dB and the resonance frequency was 9.66 GHz when $\varphi = 0°$. When $\varphi = 45°$, the

Table 1 The Q-factors with various incident angles.

7.60 GHz	Incident angle	0°	15°	30°	45°	60°
	Q-factors	6.38	6.55	7.13	8.71	12.70
10.27 GHz	Incident angle	0°	15°	30°	45°	60°
	Q-factors	14.26	14.67	16.03	19.37	26.17

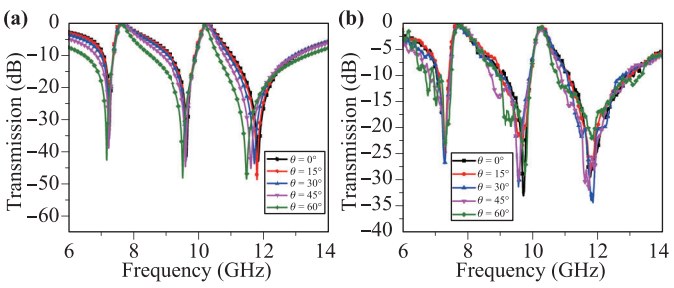


Fig. 5 Transmission spectra for different incident angles. **(a)** Simulation; **(b)** Experiment.

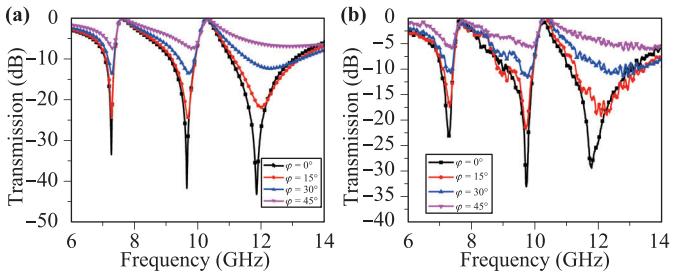


Fig. 6 Transmission spectra for different polarizing angles. **(a)** Simulated; **(b)** Measured.

resonance frequency moved to 9.84 GHz, and the corresponding transmission coefficient was −7.44 dB. The first and third transmission dips have the same variation tendency and resonance frequencies, and the transmission coefficients of two transparency peaks remain unchanged. In Fig. 6(b), the measured results are in agreement with the simulated results. The resonance frequencies of the two transparency peaks do not vary far from around 7.67 and 10.25 GHz. The amplitudes of the three dips are higher than those for the simulation results at different polarizing angles. However, the transmission spectra show an identical frequency variation trend to that in the simulation.

To elaborate on the coupling process of the proposed E–ε metamaterial, the surface current distribution and the magnetic field are depicted in Figs. 7 and 8, respectively. We employed the same amplitude scale separately that make all results accomplishing a correct comparison in Figs. 7 and 8. The surface current distributions chosen correspond to the two transparency peaks and three transmission dips: 7.60 and 10.27 GHz, and 7.27, 9.66 and 11.85 GHz, respectively. At 7.60 GHz, the surface current mainly concentrates on the ring around ε-shaped and E-shaped patterns, taking the form of a magnetic dipole. Meanwhile, the surface current in two transverse lines flows in the opposite direction. Figure 7(b) shows the distribution of the surface current at 10.27 GHz. In

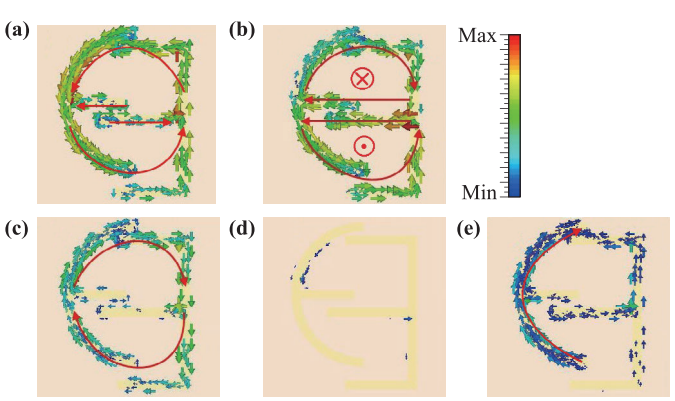


Fig. 7 The distribution of the surface current. **(a)** 7.60 GHz. **(b)** 10.27 GHz. **(c)** 7.27 GHz. **(d)** 9.66 GHz. **(e)** 11.85 GHz.

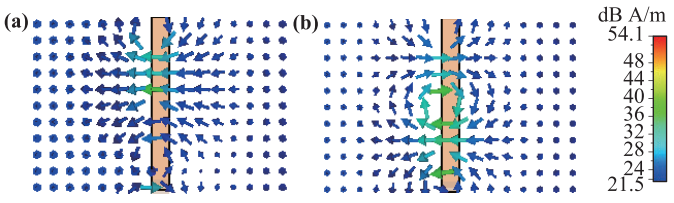


Fig. 8 The magnetic fields. **(a)** 7.60 GHz; **(b)** 10.27 GHz.

the ε-shaped and E-shaped patterns, it forms two looped currents in opposite directions, which is equivalent to two magnetic dipoles and interconnected head-to-tail circle. In this way, a toroidal dipole is formed. In Fig. 7(c), the surface current forms a ring, like Fig. 7(a), and the current intensity at the transparency dip is lower than that at the transparency peak. There is an almost inexistent current at 9.66 GHz, which is shown in Fig. 7(d). The surface current distribution of 11.85 GHz is depicted in Fig. 7(e), shown to concentrate on the ε-shaped part of the pattern, and is equivalent to an electric dipole.

The magnetic fields of the two transparency peaks are shown in Fig. 8. In Fig. 8(a), the magnetic field is flowing from the back of the dielectric substrate to the front metal, which can be viewed as a magnetic dipole. At 10.27 GHz, most of the magnetic field is restricted to flowing inside the dielectric substrate and forms a closed circular magnetic current, which is shown in Fig. 8(b). It is considered as a toroidal dipole.

The radiated power of multipoles is an important method in the quantitative analysis of the EIT-like metamaterial coupling mechanism. The calculation formulas of the radiated power of multipoles are based on the conducting current density j and are given as

$$P = \frac{1}{\mathrm{i}\omega}\int j\mathrm{d}^3 r, \tag{1}$$

$$M = \frac{1}{2c}\int (r\times j)\mathrm{d}^3 r, \tag{2}$$

$$T = \frac{1}{10c}\int [(r\cdot j)r - 2r^3 j]\mathrm{d}^3 r, \tag{3}$$

$$Q^{(m)}_{\alpha,\beta} = \frac{1}{3c}\int [(r\times j)_\alpha r_\beta + (r\times j)_\beta r_\alpha \mathrm{d}^3 r, \tag{4}$$

where j is the induced current density, c is the speed of light in vacuum, ω is the frequency and r is the distance vector from the origin to point (x, y, z) in a Cartesian coordinate system $(\alpha, \beta = x, y)$. Therefore, the decomposed far-field scatter power by these multipole moments can be calculated using the following equations [34]:

$$I_P = \frac{2\omega^4}{3c^3}|P|^2, \tag{5}$$

$$I_M = \frac{2\omega^4}{3c^3}|M|^2, \tag{6}$$

$$I_T = \frac{2\omega^6}{3c^5}|T|^2, \tag{7}$$

$$I_{M_e} = \frac{\omega^6}{20c^5}|M_e|^2. \tag{8}$$

Eqs. (5)–(8) give the radiated power of the electric, magnetic, and toroidal dipoles and magnetic quadrupole, respectively. The calculation results for the radiated power of the multipoles are exhibited in Fig. 9. We can observe that the radiated powers of the electric and magnetic dipoles decline at 7.60 and 10.27 GHz. When it comes to the magnetic quadrupole, it significantly increases in the two transparency peaks. However, the change of toroidal dipole is very clear: firstly, there are two deep dips at 7.27 and 11.85 GHz, and additionally, two strong toroidal dipole responses appear in the two transparency peaks. The toroidal dipole is lower at 7.60 GHz and is larger at 10.27 GHz, as shown in Fig. 9. At 9.66 GHz, the radiated power of the toroidal dipole drops to the lowest point between 7.60 and 10.27 GHz. This manifests that coupling between electric and toroidal dipole can generate an EIT-like material.

Refractive index sensors are a common application for EIT-like metamaterials and have potential applications in environment sensing. Sensitivity (S) is a basic parameter to indicate the performance of a sensor. It is calculated by dividing the shift frequency by the refractive index unit (RIU) [35]. The simulation results of various refractive indexes are presented in Fig. 10. Here, the refractive index ranges from 1.0 to 1.5 with a step of 0.1. With an increasing refractive index, the resonance frequencies of the two transparency peaks are both red-shifted. Ultimately, formulas are utilized to determine the refractive index that affects the transparency peak's resonance frequency and are based on the resonance frequency (the first transparency peak f_1 and the second transparency peak f_2) and refractive index n, as shown below:

$$f_1 = 0.99587n + 7.58619, \tag{9}$$

$$f_2 = 0.98812n + 10.2681. \tag{10}$$

The resonance frequencies of different refractive indexes and transparency peaks of the simulation results can be

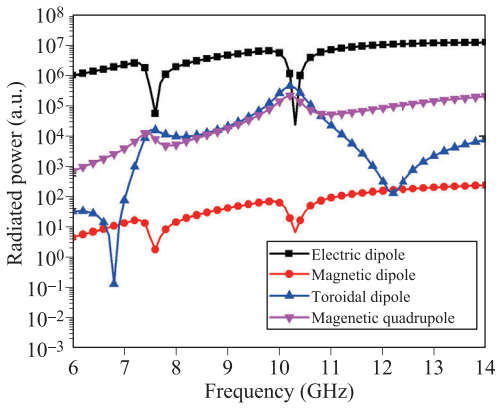


Fig. 9 Radiated power of electric, magnetic, and toroidal dipoles.

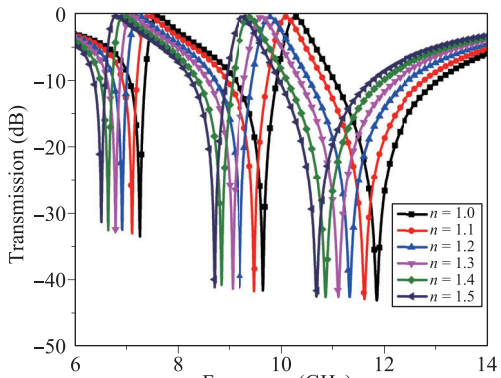


Fig. 10 Transmission spectra for different refractive indexes.

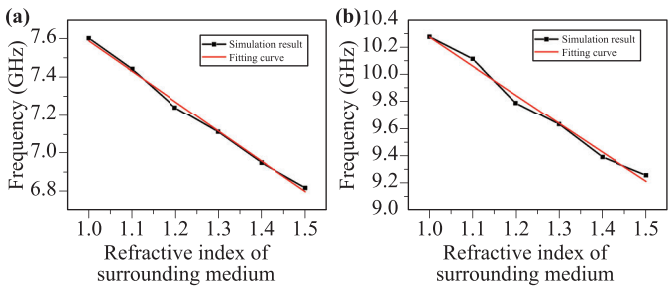


Fig. 11 The fitting curves for different refractive indexes and resonance frequencies. **(a)** First transparency peak. **(b)** Second transparency peak.

observed in Fig. 11. At the first transparency peak, the simulation points are in agreement with the fitting curve in Fig. 11(a), in which S is 1.57 GHz/RIU. The simulation points of Fig. 11(b) show a little deviation from the fitting curve. The S of the second transparency peak is 2.10 GHz/RIU.

4 Conclusions

In conclusion, an E–ε metamaterial with dual-band EIT is proposed, where the destructive interference between the electric and toroidal dipoles can generate EIT. The distribution of the surface current and the magnetic field verify the electric and toroidal dipoles. The radiated power of the multipoles reveals that the toroidal dipole response is weaker than the electric dipole response in the first transparency peak and stronger than the electric dipole response in the second transparency peak. The experimental results are in agreement with the simulation results. The proposed E–ε metamaterial can be used to achieve refractive index sensing of the surrounding medium, which will have potential applications in various civilian and military products.

Acknowledgements This work was supported by the National Natural Science Foundation of China (Grant Nos. 61741104 and

61701206), the Self-determined Research Funds of Central China Normal University from the Colleges' Basic Research and Operation of Ministry of Education of China (Grant Nos. CCNU18GF004 and CCNU18JCXK02), and the Funding for Basic Scientific Research Business of Central Universities (Innovation Funding Project) (Grant No. 2018CXZZ116).

References

1. J. Hao, M. Qiu, and L. Zhou, Manipulate light polarizations with metamaterials: From microwave to visible, *Front. Phys. China* 5(3), 291 (2010)
2. C. R. Simovski, P. A. Belov, A. V. Atrashchenko, and Y. S. Kivshar, Wire metamaterials: Physics and applications, *Adv. Mater.* 24(31), 4229 (2012)
3. Z. Shen, H. Yang, X. Huang, and Z. Yu, Design of negative refractive index metamaterial with water droplets using, *J. Opt.* 19(11), 115101 (2017)
4. H. Chen, L. Ran, J. Huangfu, X. Zhang, K. Chen, T. M. Grzegorczyk, and J. Au Kong, Left-handed materials composed of only S-shaped resonators, *Phys. Rev. E* 70(5), 057605 (2004)
5. Z. Shen, X. Huang, H. Yang, T. Xiang, C. Wang, Z. Yu, and J. Wu, An ultra-wideband, polarization insensitive, and wide incident angle absorber based on an irregular metamaterial structure with layers of water, *J. Appl. Phys.* 123(22), 225106 (2018)
6. G. Y. Song, W. X. Jiang, Q. Cheng, L. T. Wu, H. Y. Dong, and T. J. Cui, Acoustic magnifying lens for far-field high resolution imaging based on transformation acoustics, *Adv. Mater. Technol.* 2(9), 1700089 (2017)
7. Z. L. Mei and T. J. Cui, Transparent shells-invisible to electromagnetic waves, *Prog. Electromagn. Res. B* 18, 149 (2009)
8. S. Sui, H. Ma, J. Wang, Y. Pang, and S. Qu, Topology optimization design of a lightweight ultra-broadband wide-angle resistance frequency selective surface absorber, *J. Phys. D Appl. Phys.* 48(21), 215101 (2015)
9. J. Wu, P. Wang, X. J. Huang, F. Rao, X. Y. Chen, Z. Y. Shen, and H. L. Yang, Design and validation of liquid permittivity sensor based on RCRR microstrip metamaterial, *Sens. Actuators A Phys.* 280, 222 (2018)
10. M. Kraft, Y. Luo, S. A. Maier, and J. B. Pendry, Designing plasmonic gratings with transformation optics, *Phys. Rev. X* 5(3), 031029 (2015)
11. Y. Luo, D. Y. Lei, S. A. Maier, and J. B. Pendry, Transformation-optics description of plasmonic nanostructures containing blunt edges/corners: From symmetric to asymmetric edge rounding, *ACS Nano* 6(7), 6492 (2012)
12. Y. Y. Fu, Y. D. Xu, and H. Y. Chen, Negative refraction based on purely imaginary metamaterials, *Front. Phys.* 13(4), 134206 (2018)
13. K. Marinov, A. D. Boardman, V. A. Fedotov, and N. Zheludev, Toroidal metamaterial, *New J. Phys.* 9(9), 324 (2007)
14. I. B. Zel'dovich, Electromagnetic interaction with parity violation, *Sov. J. Exp. Theor. Phys.* 6, 1184 (1958)
15. A. A. Basharin, V. Chuguevsky, N. Volsky, M. Kafesaki, and E. N. Economou, Extremely high Q-factor metamaterials due to anapole excitation, *Phys. Rev. B* 95(3), 035104 (2017)
16. H. Jiang, W. Zhao, and Y. Jiang, Frequency-tunable and functionality-switchable polarization device using silicon strip array integrated with a graphene sheet, *Opt. Mater. Express* 7(12), 4277 (2017)
17. N. Papasimakis, V. A. Fedotov, V. Savinov, T. A. Raybould, and N. I. Zheludev, Electromagnetic toroidal excitations in matter and free space, *Nat. Mater.* 15(3), 263 (2016)
18. T. Xiang, T. Lei, S. Hu, J. Chen, X. Huang, and H. Yang, Resonance transparency with low-loss in toroidal planar metamaterial, *J. Appl. Phys.* 123(9), 095104 (2018)
19. S. S. Li, J. B. Yuan, and L. M. Kuang, Coherent manipulation of spin squeezing in atomic Bose-Einstein condensate via electromagnetically induced transparency, *Front. Phys.* 8(1), 27 (2013)
20. M. Liu, Q. Yang, Q. Xu, X. Chen, Z. Tian, J. Gu, C. Ouyang, X. Zhang, J. Han, and W. Zhang, Tailoring mode interference in plasmon-induced transparency metamaterials, *J. Phys. D Appl. Phys.* 51(17), 174005 (2018)
21. J. Zhang, S. Xiao, C. Jeppesen, A. Kristensen, and N. A. Mortensen, Electromagnetically induced transparency in metamaterials at near-infrared frequency, *Opt. Express* 18(16), 17187 (2010)
22. W. Zhao, S. Wang, B. Liu, I. Verzhbitskiy, S. Li, F. Giustiniano, D. Kozawa, K. P. Loh, K. Matsuda, K. Okamoto, R. F. Oulton, and G. Eda, Exciton-plasmon coupling and electromagnetically induced transparency in monolayer semiconductors hybridized with Ag nanoparticles, *Adv. Mater.* 28(14), 2709 (2016)
23. Z. Y. Shen, T. Y. Xiang, J. Wu, Z. T. Yu, and H. L. Yang, Tunable and polarization insensitive electromagnetically induced transparency using planar metamaterial, *J. Magn. Magn. Mater.* 476, 69 (2019)
24. T. Liu, H. Wang, Y. Liu, L. Xiao, C. Zhou, Y. Liu, C. Xu, and S. Xiao, Independently tunable dual-spectral electromagnetically induced transparency in a terahertz metal – graphene metamaterial, *J. Phys. D Appl. Phys.* 51(41), 415105 (2018)
25. Z. Y. Shen, T. Y. Xiang, N. Wu, J. Wu, Y. Tian, and H. L. Yang, Dual-band electromagnetically induced transparency based on electric dipole-quadrupole coupling in metamaterials, *J. Phys. D Appl. Phys.* 52(1), 015003 (2019)
26. S. Hu, D. Liu, and H. L. Yang, Electromagnetically induced transparency in an integrated metasurface based on bright-dark-bright mode coupling, *J. Phys. D Appl. Phys.* 52(17), 175305 (2019)
27. J. Zhang and A. Zayats, Multiple Fano resonances in single-layer nonconcentric core-shell nanostructures, *Opt. Express* 21(7), 8426 (2013)

28. V. A. Fedotov, A. V. Rogacheva, V. Savinov, D. P. Tsai, and N. I. Zheludev, Resonant transparency and non-trivial non-radiating excitations in toroidal metamaterials, *Sci. Rep.* 3(1), 2967 (2013)

29. L. Y. Guo, M. H. Li, X. J. Huang, and H. L. Yang, Electric toroidal metamaterial for resonant transparency and circular cross-polarization conversion, *Appl. Phys. Lett.* 105(3), 033507 (2014)

30. S. Han, L. Cong, F. Gao, R. Singh, and H. Yang, Observation of Fano resonance and classical analog of electromagnetically induced transparency in toroidal metamaterials, *Ann. Phys.* 528(5), 352 (2016)

31. M. Gupta, V. Savinov, N. Xu, L. Cong, G. Dayal, S. Wang, W. Zhang, N. I. Zheludev, and R. Singh, Sharp toroidal resonances in planar terahertz metasurfaces, *Adv. Mater.* 28(37), 8206 (2016)

32. L. Zhu, L. Dong, J. Guo, F. Meng, J. He, C. H. Zhao, and Q. Wu, A low-loss electromagnetically induced transparency (EIT) metamaterial based on coupling between electric and toroidal dipoles, *RSC Advances* 7(88), 55897 (2017)

33. L. Cong, V. Savinov, Y. K. Srivastava, S. Han, and R. Singh, A metamaterial analog of the Ising model, *Adv. Mater.* 30(40), 1804210 (2018)

34. M. Gupta, Y. K. Srivastava, and R. Singh, A toroidal metamaterial switch, *Adv. Mater.* 30(4), 1704845 (2018)

35. Y. Tian, S. Hu, X. J. Huang, Z. T. Yu, H. Lin, and H. L. Yang, Low-loss planar metamaterials electromagnetically induced transparency for sensitive refractive index sensing, *J. Phys. D Appl. Phys.* 50(40), 405105 (2017)